A&A 423, 1119–1131 (2004)
DOI: 10.1051/0004-6361:20040259

Astronomy & Astrophysics

Evolution and magnetic topology of the M 1.0 flare of October 22, 2002

A. Berlicki[1,2], B. Schmieder[1,3], N. Vilmer[1], G. Aulanier[1], and G. Del Zanna[4]

[1] Observatoire de Paris, Section de Meudon, LESIA, 92195 Meudon Principal Cedex, France
e-mail: arkadiusz.berlicki@obspm.fr
[2] Astronomical Institute of the Wrocław University, ul. Kopernika 11, 51-622 Wrocław, Poland
[3] Institute of Theoretical Astrophysics, University of Oslo, Blindern, 0315 Oslo, Norway
[4] DAMTP, University of Cambridge, Cambridge, UK

Received 12 February 2004 / Accepted 30 April 2004

Abstract. In this paper we analyse an M 1.0 confined flare observed mainly during its gradual phase. We use the data taken during a coordinated observational campaign between ground based instruments (THEMIS and VTT) and space observatories (SoHO/CDS and MDI, TRACE and RHESSI). We use these multi-wavelength observations to study the morphology and evolution of the flare, to analyse its gradual phase and to understand the role of various heating mechanisms. During the flare, RHESSI observed emission only within the 3–25 keV spectral range. The RHESSI spectra indicate that the emission of the flare was mainly of thermal origin with a small non-thermal component observed between 10 and 20 keV. Nevertheless, the energy contained in the non-thermal electrons is negligible compared to the thermal energy of the flaring plasma. The temperature of plasma obtained from the fitting of the RHESSI X-ray spectra was between 8.5 and 14 MK. The lower temperature limit is typical for a plasma contained in post flare loops observed in X-rays. Higher temperatures were observed during a secondary peak of emission corresponding to a small impulsive event. The SoHO/CDS observations performed in EUV Fe XIX line also confirm the presence of a hot plasma at temperatures similar to those obtained from RHESSI spectra. The EUV structures were located at the same place as RHESSI X-ray emission. The magnetic topology analysis of the AR coming from a linear force-free field extrapolation explains the observed features of the gradual phase of the flare i.e. the asymmetry of the ribbons and their fast propagation. The combination of the multi-wavelength observations with the magnetic model further suggests that the onset of the flare would be due to the reconnection of an emerging flux in a sheared magnetic configuration.

Key words. Sun: flares – Sun: X-rays, γ-rays – Sun: magnetic fields

1. Introduction

The gradual phase of flares can last half an hour to a few hours. Detailed observations of flares during their gradual phase have been recorded by the Solar Maximum Mission (SMM) and later by Yohkoh (Švestka et al. 1982; Schmieder et al. 1996, 1997; van Driel et al. 1997). Soft X-ray instruments in these missions observed the formation of hot loops (10–20 MK). These loops subsequently cool and become visible as post-flare loops in lower temperatures (EUV and Hα lines). The hot loops are formed at higher and higher altitudes with time. Such events were interpreted with models based on the Kopp & Pneuman (1976) concept. These models exist also in two dimensions (Forbes & Malherbe 1986; Forbes & Acton 1996). During the gradual phase of flares, magnetic field lines reconnect at an X point or neutral sheet in the corona. Particles are accelerated as a consequence of the reconnection. Plasma in the loop is heated and "gentle" chromospheric evaporation can occur at the footpoints of the loops in high density plasma region. These models are well adapted for the interpretation of flare events in general, not only for eruptive two ribbon flares, but also for confined flares (Švestka 1986) that are due to magnetic reconnection at (quasi-) separatrix layers (Démoulin et al. 1997) and which do not result in an eruption.

During the reconnection process and the gradual phase of flares, SMM with its HXIS telescope could image the plasma heated by high energy particles in four energy bands of spectra with a low spatial resolution. The Hard X-ray telescope onboard Yohkoh had a better spatial resolution but no low energy band. A long debate about the long duration emission of particles continues to understand if the particles accelerated during the impulsive phase were trapped at the reconnection point or if they were continuously accelerated.

To distinguish between both processes and to further investigate this question we use the X-ray observations obtained with high spectral resolution in the 3–20 keV range by the Reuven Ramaty High Energy Solar Spectroscopic Imager (RHESSI: Lin et al. 2002). RHESSI was launched in 2002 and continues to operate observing the solar spectrum in the energy range 3 keV–17 MeV.

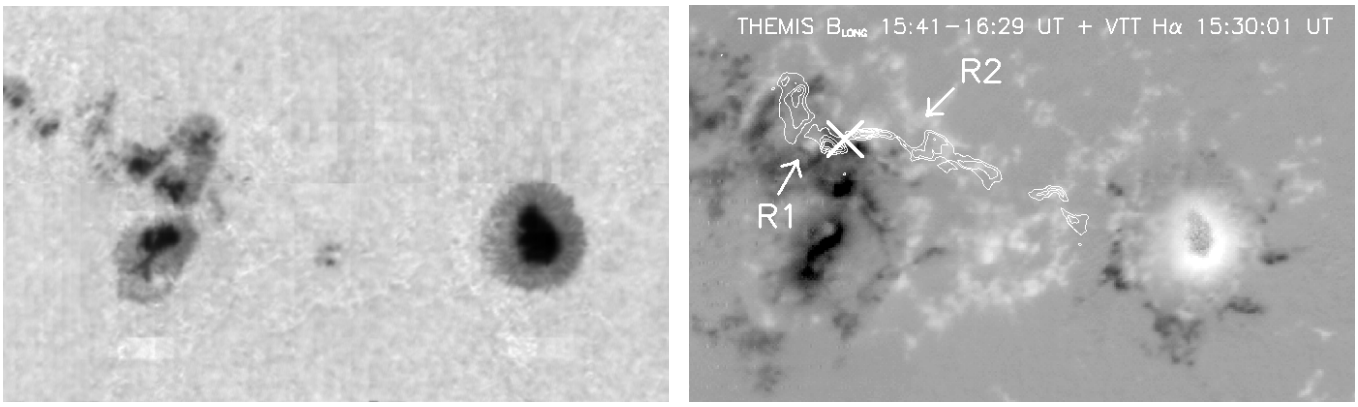

Fig. 1. Image of AR 0162 obtained from THEMIS/MSDP observations taken between 15:41 and 16:29 UT in the Na I D_1 spectral line wing at 200 mÅ from the line centre (*left panel*). In the right panel we present the line-of-sight (LOS) magnetic field deduced from *I* and *V* Stokes profiles at 100 mÅ from the Na I D_1 line centre overlaid with the contours of the Hα flare observed by VTT/MSDP at 15:30:01 UT. The field-of-view (FOV) is $400'' \times 250''$. The cross denotes the place separating two main ribbons R1 and R2.

We performed multi-wavelength observations of a long duration M 1.0 flare during a coordinated observational campaign between ground based instruments (THEMIS and VTT) and space observatories (SoHO/CDS and MDI, TRACE and RHESSI). The flare was followed by several local increases of X-ray emission in its decay phase. The flare occurs in a mainly bipolar active region (as observed by THEMIS). Looking at SoHO/EIT and LASCO data, we noticed that neither coronal mass ejection nor any related coronal signature of eruptive events (such as transient coronal dimming and fast propagating wave-like disturbance) were associated with the flare. Therefore, this event was certainly a confined flare. We observe mainly one long bright ribbon in Hα and with the Transition Region and Corona Explorer (TRACE) at 195 Å. To understand the magnetic configuration of the flare we have performed magnetic extrapolations using the *lfff* (linear force-free field) code developed by Démoulin et al. (1997). The three-dimensional analysis of the extrapolation allows us to have a good idea of the topology of the flare. Long low sheared horizontal field lines were drawn, that may correspond to the TRACE loops. RHESSI and CDS Fe XIX images show elongated emissions over these field lines. This agrees with the models of gradual phase already explained above. The analysis of the RHESSI spectra allowed us to determine if non-thermal particles can still exist during the gradual phase of the flares.

The paper is organized as follows. In Sect. 2 we describe the observations and their coalignment. In the third section we discuss on the topology of the flare using *lfff* extrapolation. Section 4 provides description of the RHESSI X-ray spectral observations of the flare. In this section we also discussed the nature of X-ray emission. Section 5 summarizes our analysis and provides a description of our results.

2. Observations

The M 1.0 flare was observed in the NOAA 0162 active region (AR) located about N26 E21 on October 22, 2002. This active region was a target during the coordinated SoHO and ground-based observational campaign in October 2002. The active region campaign included EUV spectral observations with the SoHO/CDS Normal Incidence Spectrometer (NIS) (Harrison et al. 1995). During its passage through the solar disk (17–31 October, 2002) the active region consisted of a big leading spot located in a positive magnetic field polarity and a cluster of following spots of negative magnetic field polarity (Fig. 1).

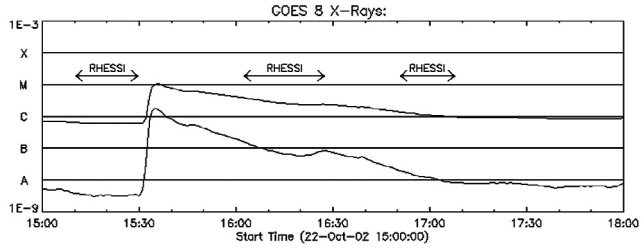

Fig. 2. Time evolution of GOES X-ray flux observed during the flare of October 22, 2002. The timings of the RHESSI observations (three orbits) are indicated. THEMIS observed continuously between 15:41–17:35 UT. TRACE and VTT/MSDP observations were performed during whole flare.

In the X-ray range, this flare was observed by GOES 8 and in its decay phase by one of the RHESSI orbits (see Fig. 2). According to the GOES 8 flux curve, the flare onset was at 15:29 UT and the 1–8 Å X-ray flux reached its maximum at 15:36 UT. During the decay phase, several local increases of the X-ray flux were observed, the most notable one with a peak at 16:28 UT.

2.1. Summary of the data

Within the X-ray spectral range, the most interesting observations were those obtained by RHESSI during the orbit between 16:03–16:28 UT. At this time the X-ray emission was detected from 3 keV to about 25 keV.

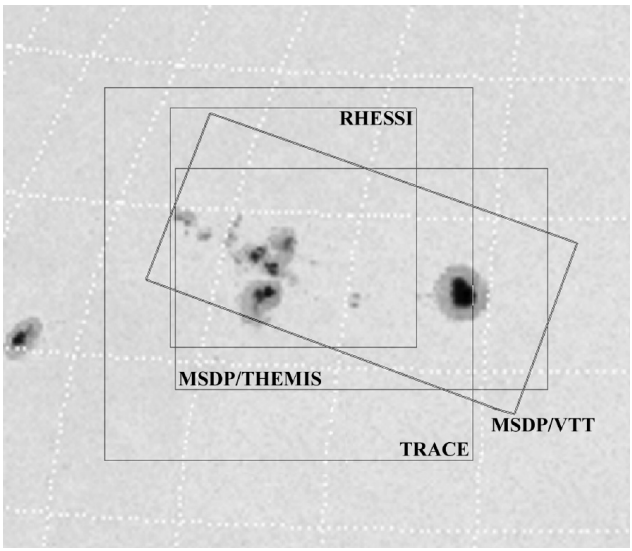

Fig. 3. Approximate orientation of FOVs of different observations used in the analysis of the flare of October 22, 2002. North is up. For RHESSI we marked the part of FOV which was used in our analysis.

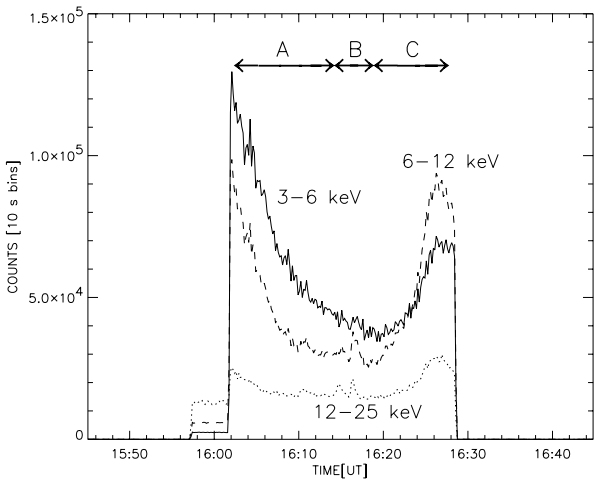

Fig. 4. Time evolution of RHESSI X-ray counts rates observed during the flare of October 22, 2002 in 3–6, 6–12 and 12–25 keV energy bands. The counts rates observed in 12–25 keV energy band were multiplied by a factor of 10 to make the plots more clear. Letters A, B and C denote the phases in the X-ray flux evolution (see Sect. 2.3).

The spectro-polarimetric observations of the AR 0162 were performed with the THEMIS telescope, operating in the MSDP (Multichannel Subtractive Double Pass spectrograph) observing mode (Mein 2002).

In our analysis we also used the VTT/MSDP observations in the Hα line (Mein 1991). During the flare between 15:30 and 16:17 UT we completed 9 scans of the MSDP entrance window covering the whole active region with a field-of-view (FOV) of about $380'' \times 170''$.

TRACE (Handy et al. 1999) obtained high cadence (40 s) filtergrams in the 195 Å band between 15:29 and 15:41 UT (with a FOV $384'' \times 384''$ and a $1''$ resolution). Before and after this time the TRACE observations were obtained with slightly lower time resolution (50 s) and larger FOV ($512'' \times 512''$). The solar coordinates of the TRACE images were corrected by using the SoHO/EIT and MDI maps. In the EUV spectral range this flare was also observed by the SoHO/CDS instrument. In Fig. 3 we present the relative pointings and approximate fields-of-view of the various instruments used in our analysis.

2.2. Magnetic field observation

On October 22, 2002 the spectro-polarimetric observations of the AR 0162 were performed with the THEMIS telescope, operating in the MSDP spectrograph observing mode. THEMIS is a polarization-free telescope, designed especially for polarimetric observations. The polarization analyser provides successively the Stokes parameters $I \pm S$ ($S = V$, Q or U) without differential blurring due to seeing effects. Detailed descriptions of the specific instrumental set-up of THEMIS in the MSDP observing mode can be found in Mein (2002).

During the flare the observations in the Na I D_1 sodium line were performed only for $S = V$ and we obtained the Stokes I and V profiles simultaneously in the 16 MSDP channels. The line-of-sight (LOS) magnetic field can be estimated from the observed Stokes profiles. The center-of-gravity method (Semel 1967) was used to determine the magnetic field. In this method the longitudinal (or LOS) component B_l of the magnetic field is proportional to the relative shift between the centres of $I + V$ and $I - V$ profiles (for details see the paper Eibe et al. 2002).

On October 22, 2002 we obtained five scans of the AR 0162 during the flare. Each scan lasted about 25 min. From these scans five sets of data were reconstructed. Each set of data consists of the images ($600'' \times 130''$) in the Na D_1 sodium line (intensity, velocity and LOS magnetic field maps at different wavelengths). The FOV of the THEMIS scans was too small to cover the whole active region and to make an image of the whole AR thus we needed to perform two scans with two different FOV. On October 22, 2002 THEMIS observations of the AR 0162 were performed from about 10:18 until 18:00 UT. Analysis of all images showed that there were no significant changes of LOS magnetic field configuration during the day. Finally, from five scans we obtained two full images ($400'' \times 250''$) of the AR during the flare at 15:41–16:29 and 16:47–17:35 UT. The pixel size of these images is $0.25''$ but the spatial resolution of the images was limited by seeing (about $1''$).

Figure 1 presents THEMIS observations of AR 0162 obtained in the Na I D_1 spectral line wing at 200 mÅ from the line centre (left panel). In the right panel we present the LOS magnetic field deduced from I and V Stokes profiles of the Na I D_1 line overlaid with the isophotes of the Hα flare observed by VTT/MSDP. The area of high Hα emission (more concentrated isophotes) is located close to the emerging bipole – a two polarity emerging flux of high gradient magnetic field (see Sect. 3).

2.3. X-ray observations

The decay phase of this flare was observed by RHESSI during the orbit between 16:03–16:28 UT (Fig. 4). From RHESSI

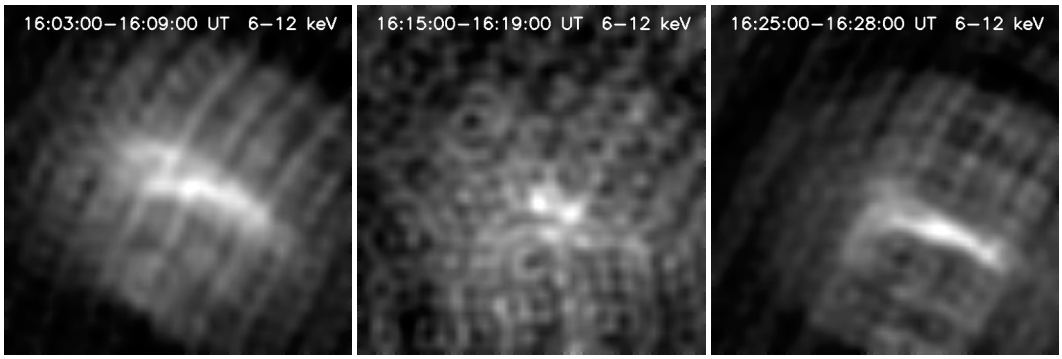

Fig. 5. Sequence of RHESSI images (224″ × 224″) reconstructed in 6–12 keV energy band during the gradual phase of the flare on October 22, 2002.

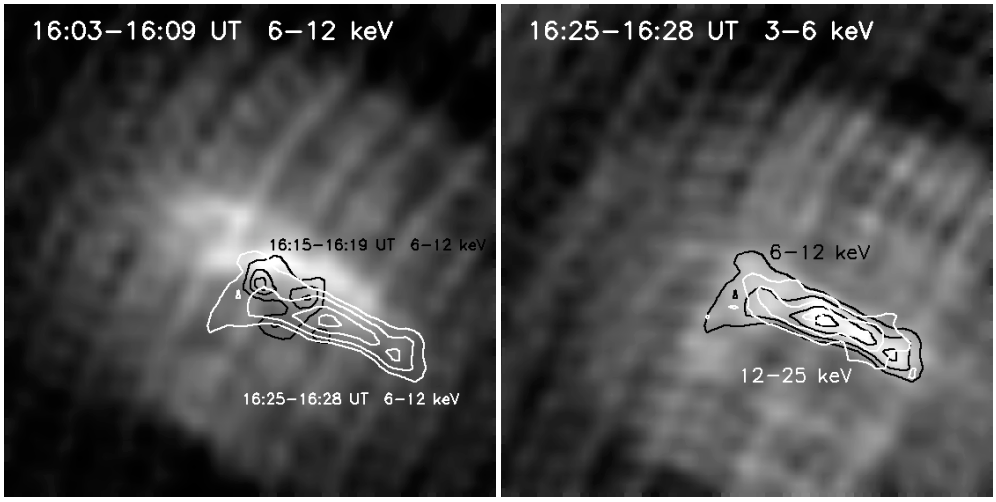

Fig. 6. *Left panel*: the time evolution of RHESSI X-ray structures observed in 6–12 keV energy band. RHESSI image (224″ × 224″) taken at 16:03–16:09 UT is overlaid with the X-ray contours at 16:15–16:19 and 16:25–16:28 UT. Right panel: RHESSI images between 16:25 and 16:28 UT observed in three different (3–6, 6–12 and 12–25 keV) energy band. The image shows the X-ray structures observed in 3–6 keV energy bands overlaid with the contours of the structures observed at this time in 6–12 and 12–25 keV energy bands.

data, it is possible to construct images in some chosen energy bands, and to build low-resolution spectra. During the decay phase the count rates detected from 3 keV to 25 keV were sufficiently high to make images with a spatial resolution of 4″ but it was necessary to accumulate count rates over a few minutes to reconstruct the images with sufficient quality. We obtained the images in three energy bands 3–6 keV, 6–12 keV and 12–25 keV using the CLEAN algorithm and front collimators 3F–9F. During this flare there was no attenuator in front of the grids. We concentrated the analysis of the RHESSI data on three periods of time (ranges A, B, C in Fig. 4). During the period A (16:03–16:13 UT), the X-ray count rates exhibited a continuous decrease. At 16:16 UT a weak increase of the count rates in 6–12 and 12–25 keV bands, lasting about 2 min, was observed (range B). This small event was not visible on the RHESSI flux curves for higher energies. After it, from about 16:18 UT we can see a continuous increase of the X-ray flux (range C). It reached its maximum at about 16:26 UT, just before the passage of RHESSI through the radiative belts.

Between 16:03 and 16:09 UT during the decaying X-ray flux (range A) we could reconstruct the images only in the 3–6 and 6–12 keV energy bands (Fig. 5 – left panel). The images show an elongated loop-like structure with the same shape both in the 3–6 keV and in the 6–12 keV range. We also examined the small event (period B), by reconstructing RHESSI images during its peak (16:15–16:19 UT) in the 3–6 and 6–12 keV energy bands (Fig. 5 – middle panel). The X-ray emission was concentrated in two compact sources located slightly to the south of the emission observed at 16:03 UT (Fig. 6 – left panel). In the 12–25 keV energy band the count rates were too low to make images but analysis of the spectra can be done in this range.

The following increase (period C) was clearly visible in the 3–6, 6–12 and 12–25 keV energy bands, and peaked at about 16:26 UT. We have reconstructed images around this peak (16:25–16:28 UT), shown in Fig. 5 – right panel and Fig. 6. Also in this case elongated loop-like structures are seen, that are now located to the south of the structures previously observed at 16:15–16:19 UT. There were no significant shifts between the positions of these X-ray structures as observed at different energies (Fig. 6 – right panel).

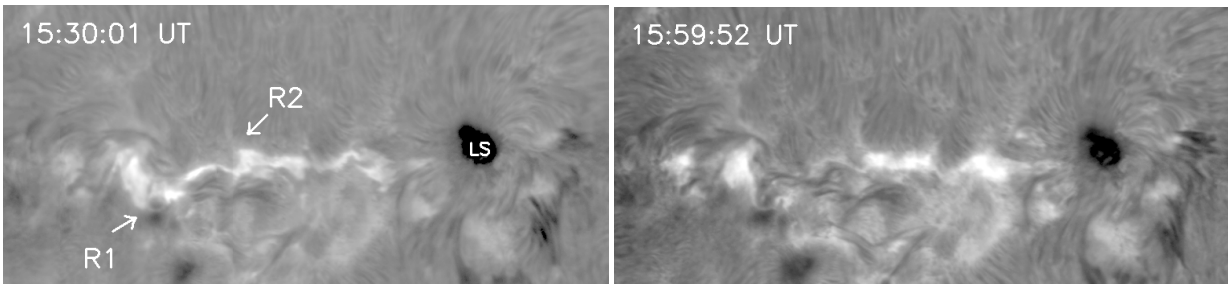

Fig. 7. The flare of October 22, 2002 observed in Hα line by the MSDP/VTT spectrograph. The FOV is $340'' \times 200''$. R1 and R2 denote the two main ribbons of the flare. LS marks the leading spot of the AR 0162.

2.4. Coronal Diagnostic Spectrometer (CDS)

By rastering the CDS slit (from west to east), monochromatic images and velocity maps of the FOV ($4' \times 4'$) can be constructed. The NIS observes the 305–635 Å spectral range with two gratings, and a spatial resolution of approximately $5''$. The NIS spectral range includes a large number of lines, but due to telemetry limitations, only a limited number of NIS lines are normally extracted and telemetered to the ground. For more details of the CDS see e.g. Harrison et al. (1995) and for data reduction Del Zanna et al. (2001).

Two types of NIS "rasters" were used for these observations: 1) a slow (1h 20 min), diagnostic raster that extracts many diagnostic lines; 2) a fast (20 min) raster, that only extracts a few lines, selected to cover a wide range of temperatures (He I 522.2 Å, $\log T = 4.5$; O IV 554.5 Å, $\log T = 5.3$; O V 630 Å, $\log T = 5.4$; Mg X 625 Å, $\log T = 6.0$; Si XII 520.8 Å, $\log T = 6.3$; Fe XIX 592.2 Å, $\log T = 6.9$). The two rasters used the $4'' \times 240''$ slit and were repeated a few times over the active region during the day. In this paper, only some results concerning these two CDS rasters are presented. A more detailed discussion of the CDS observations is deferred to a future paper.

NOAA 0162 was observed by CDS during the periods 08:02–13:07 UT and 15:18–18:33 UT with the two types of rasters. A relatively strong flare was observed during the fast raster taken during 12:43–13:07 UT, approximately at the same location where the M 1.0 flare took place. The M 1.0 flare that is the subject of this paper was recorded by CDS with a fast raster which scanned the active region between 15:18 and 15:43 UT. CDS also observed the same region with a diagnostic raster (15:43–17:07 UT). In our analysis we used the CDS images obtained in Fe XIX line at 592.2 Å. The CDS slit was located in the flare area during the peak X-ray emission. It should be noted that spatially-resolved EUV spectroscopic observations of flares are quite rare, although CDS has already observed a number of them, as described in Del Zanna et al. (2002a,b).

2.5. Multi-wavelength observations of the flare structure

On the Hα VTT/MSDP images well developed flare ribbons were observed from 15:30 UT. The orientation of the two main ribbons R1 and R2 suggests that the AR is sheared (Fig. 7). Hα ribbons seem to be shifted along the neutral line and they are not located opposite each other (see also Sect. 3.2). The brightest parts of Hα flare ribbons, clearly visible at 15:30 UT, were much weaker after 7 min and almost disappeared at about 15:59 UT but the other parts of the flare ribbons were still clearly visible. The two brightest parts of Hα ribbons were located in the following spot group, within the emerging bipole, each of them in an area of opposite polarity magnetic field (Fig. 1 – right panel).

The two-ribbon shape of this flare is not contradictory with its confined nature, since flare models (Démoulin et al. 1997) have shown that quasi-bipolar photospheric flux distributions can be associated with quasi-separatrix layers whose intersection with the photosphere can form only two (and not four) thin ribbons.

The first increase of emission in the 195 Å band was observed by TRACE on the image taken at 15:32:18 UT while the first increase of GOES X-ray flux of M 1.0 flare was observed at 15:29 UT. Initially, the TRACE emission was concentrated in the compact source well visible at 15:34:56 and 15:40:39 UT (Fig. 8). Later on, from about 15:58:55 UT the TRACE EUV emission was concentrated in small, rather low, thin loops spreaded along the east-west axis of the AR and in few brightenings located close to the Hα flare emission (Fig. 9 – lower panels).

In the part of the AR where the magnetic field gradient was very high the initial energy release probably took place. This idea may be supported by the TRACE 195 Å observations. In the image taken at 15:34:56 UT the brightest EUV emission was concentrated just above the emerging bipole (Fig. 8 – lower right panel) and above two bright Hα flare kernels observed at 15:30:01 UT.

The coalignment of RHESSI images with the VTT/MSDP filtergrams shows that X-ray emission observed between 16:03 and 16:09 UT is located not on the Hα flare ribbons but, in projection, it is shifted above (Fig. 9 – upper left panel). There is no shift between the emission observed in 3–6 and 6–12 keV energy bands. Later, the X-ray structures observed by RHESSI at 16:25–16:28 UT were located (in projection) in the same place as Hα flare emission observed half an hour before. In the upper right panel of Fig. 9 we present also the contours of RHESSI X-ray structures observed in three time intervals between 16:03 and 16:25 UT overlaid on THEMIS/MSDP image of LOS magnetic field. In the lower left panel of Fig. 9, the

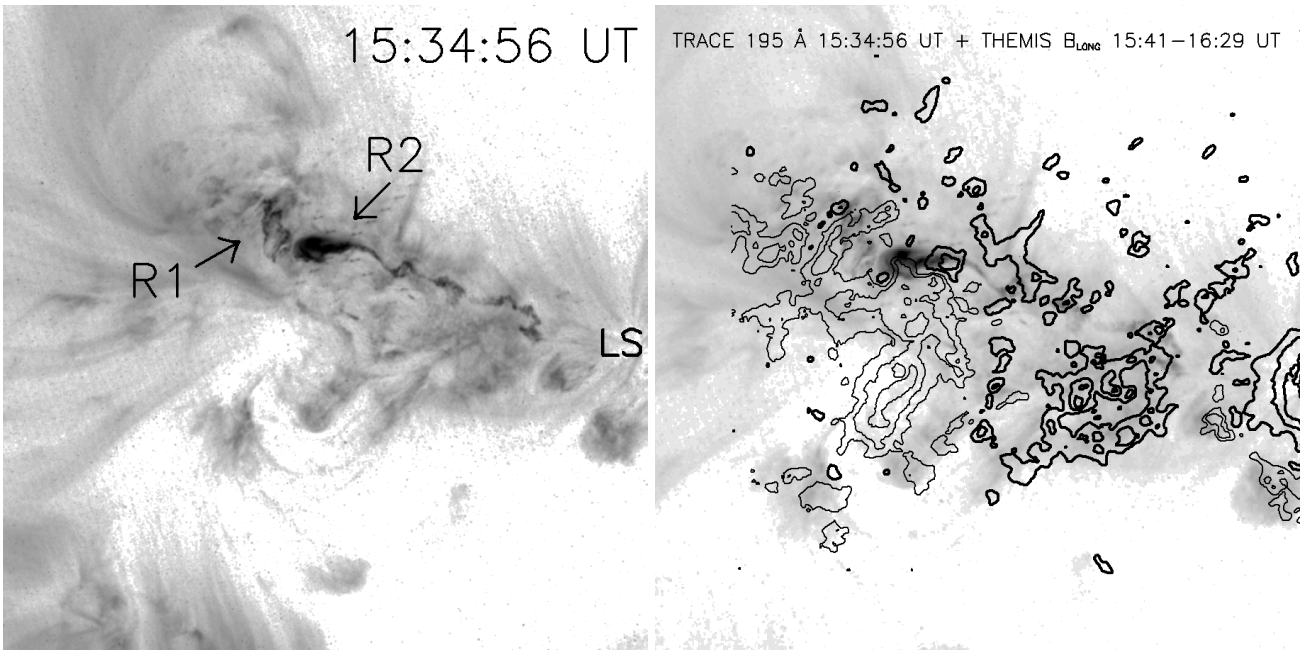

Fig. 8. TRACE 195 Å image of the AR 0162 at 15:34:56 UT. R1 and R2 denote the two main ribbons of the flare and LS marks the leading spot of the AR 0162 (*left panel*). In the right panel we present the contours of longitudinal magnetic field of the AR 0162 observed with THEMIS in the Na I D_1 spectral line at 15:41–16:29 UT. Thick and thin contours denote respectively the positive and negative polarity magnetic field.

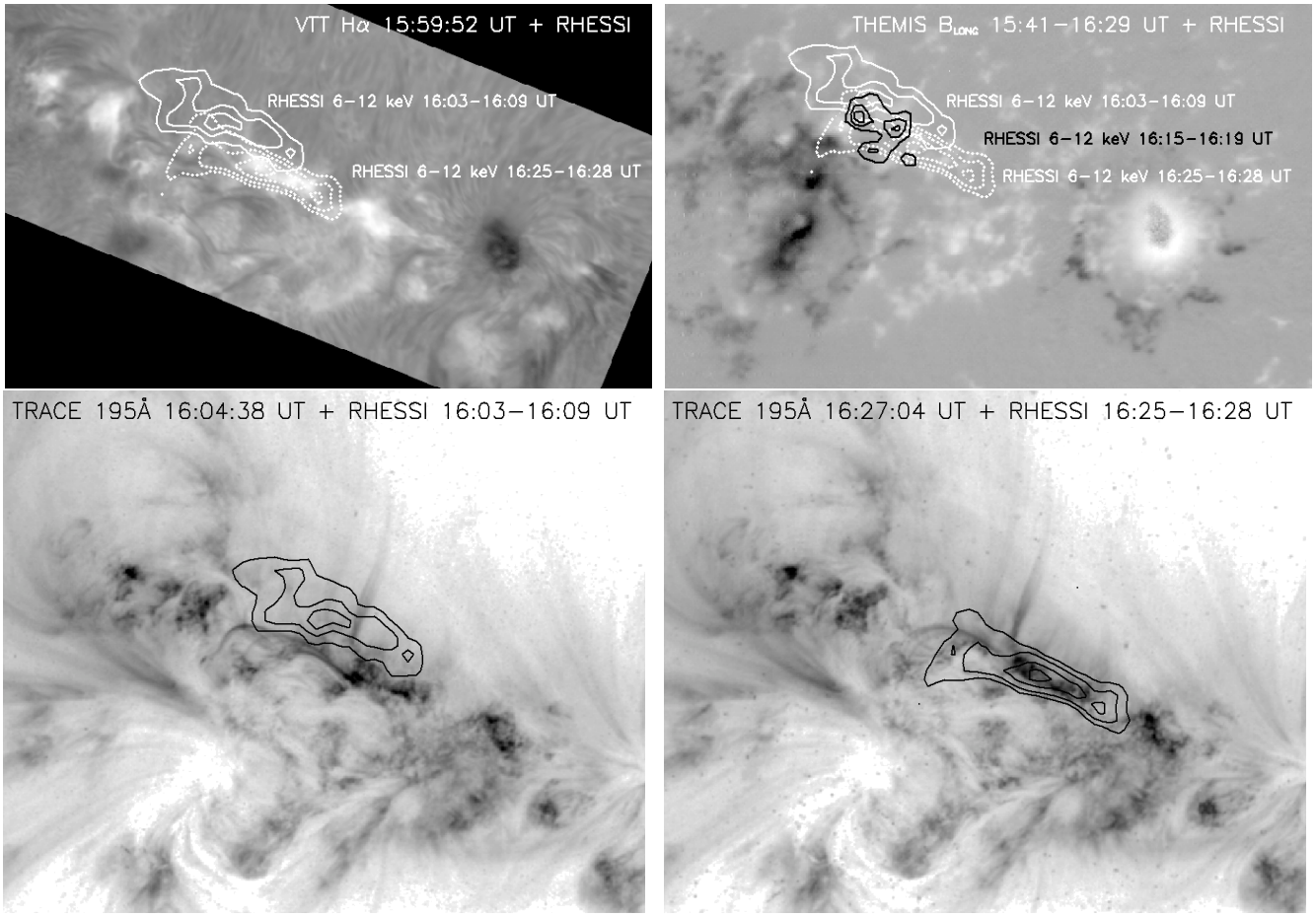

Fig. 9. VTT/MSDP image of the Hα flare in the AR 0162 at 16:00 UT (*left upper panel*) and the longitudinal magnetic field deduced from THEMIS/MSDP observations (15:41–16:29 UT) in the Na I D_1 spectral line at 100 mÅ from the line centre (*right panel*) overlaid with the contours of the X-ray structures observed by RHESSI at 16:03–16:09, 16:15–16:19 and 16:25–16:28 UT (*right upper panel*). In the lower panels we present TRACE 195 Å images of the AR 0162 (16:04:38 and 16:27:04 UT) overlaid with the contours of the X-ray structures observed by RHESSI at 16:03–16:09 and 16:25–16:28 UT time intervals.

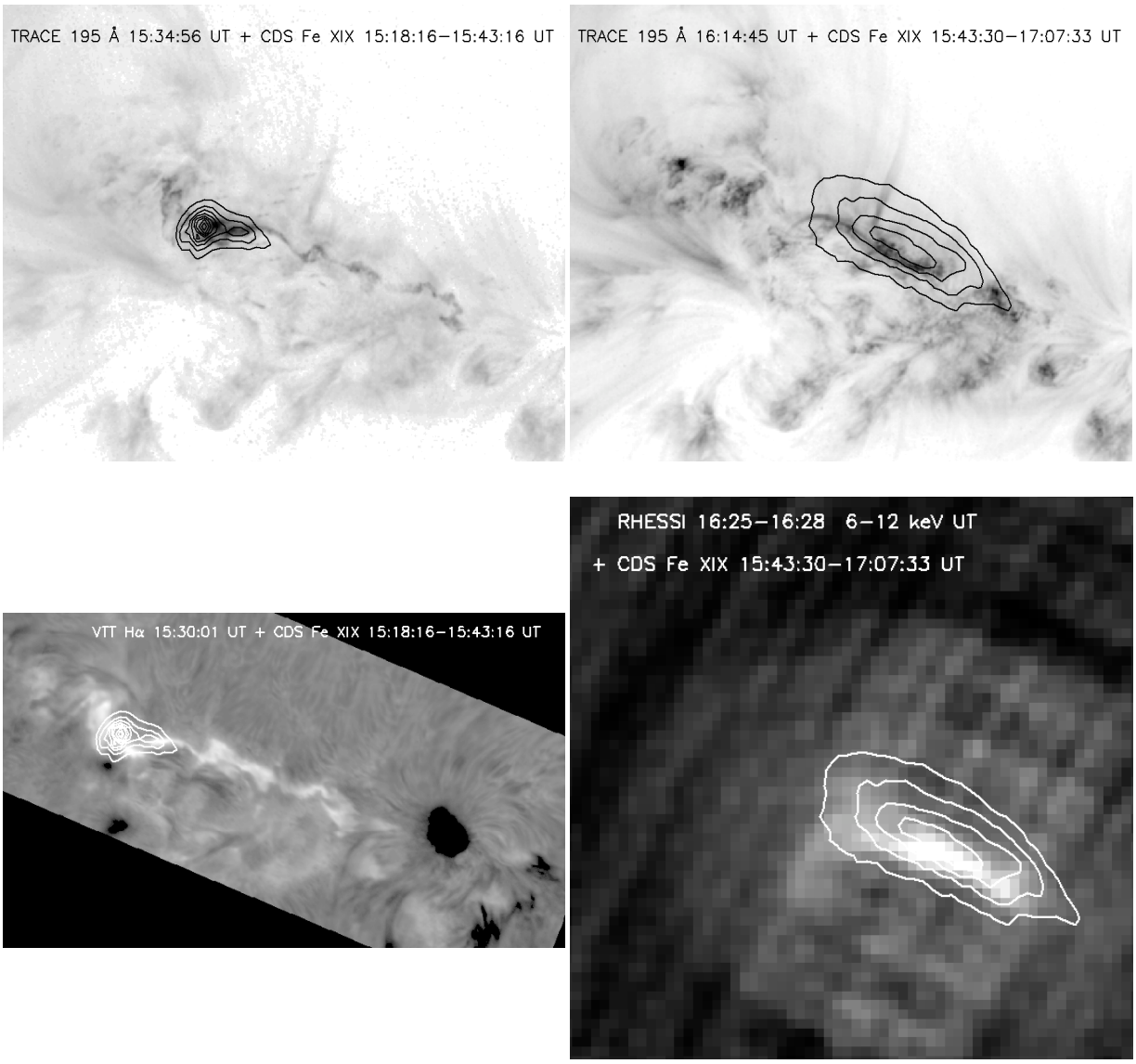

Fig. 10. TRACE 195 Å images of the AR 0162 (15:34:56 and 16:14:45 UT) overlaid with the contours of the EUV structures observed by CDS between 15:18:16–15:43:16 and 15:43:30–17:07:33 UT in the Fe XIX line (592.2 Å) (*upper panels*) and VTT/MSDP image of the Hα flare in the AR 0162 at 15:30 UT overlaid with the contours of the EUV structures observed by CDS (Fe XIX line, 592.2 Å) between 15:18:16–15:43:16 UT (*left lower panel*) and RHESSI image ($245'' \times 245''$) reconstructed for the time 16:25–16:28 UT overlaid with CDS Fe XIX structures observed between 15:43:30–17:07:33 UT (*right lower panel*).

contours of RHESSI image at 16:03–16:09 UT are overlaid on the TRACE image taken at 16:04:38 UT. Note that X-ray emission of the flare is located just above the bright thin loop-like structure seen in EUV 195 Å. Later, the X-ray emission observed by RHESSI at 16:25–16:28 UT was located (in projection) in the same place as TRACE emission observed at 16:27:04 UT (Fig. 9 – lower right panel).

During the flare, the Fe XIX line observed by CDS was very bright (reaching 3000 photon-events in the NIS detector), and clearly showed where strong heating (to at least temperatures of 8 MK) takes place. The peak emission, recorded between 15:35 and 15:43 UT, occurred just above the region of strongly mixed polarity and where the Hα flare ribbons observed by VTT/MSDP at 15:30:01 UT were located (Fig. 10 – lower left panel). The Fe XIX emission was also located just above the brightest TRACE 195 Å emission (Fig. 10 – upper left panel). Note that the TRACE 195 Å band is dominated at the flare site by Fe XXIV emission at 192.028 Å, while in general it is multithermal, with contributions from plasma at temperatures as low as 700 000 K (see Del Zanna & Mason 2003).

During the decay phase, the Fe XIX emission usually becomes more diffuse, as noted in Del Zanna et al. (2002a,b). The Fe XIX emission of the flare was recorded (Fig. 10 right panels) while the slit was covering the eastern half of the FOV, between 16:20 and 16:51 UT, i.e. the RHESSI 16:25-16:28 UT image and the CDS recording of the Fe XIX emission are almost simultaneous.

3. Interpretation of the flare ribbons in a simple topology

In this section we provide an interpretation for the triggering and the development of the confined flare by the means of a topological analysis of the coronal magnetic field above NOAA 0162 calculated from a linear force-free field model.

3.1. Linear force-free field extrapolation

For the extrapolation the LOS magnetic fields was measured with the THEMIS/MSDP in the Na I D_1 line at 12:32–13:20 UT. We used the image obtained before the flare because the FOV was extended towards the east and additional magnetic structures could be taken into account. The LOS magnetic fields were assumed to be equal to the vertical fields at the altitude $z = 0$ (i.e. $\boldsymbol{B}(x, y, z = 0)$) divided by the projection angle, as often done in extrapolations using longitudinal magnetograms only (see, e.g., Démoulin et al. 1997; Eibe et al. 2002). The extrapolation was performed in the linear force-free field approximation ($\boldsymbol{\nabla}\times\boldsymbol{B} = \alpha\boldsymbol{B}$ with $\alpha = \mathrm{cst}$) with the FFT method, so with periodic boundary conditions in (x, y) (Alissandrakis 1981). In order to minimize the boundary effects, a large computational box was chosen, with $\Delta x = \Delta y = 10^3$ Mm, and the magnetic field was computed up to $z = 150$ Mm above the photosphere. The calculation was done with $nx = ny = 1024$ mesh points so as to sufficiently resolve the emerging bipole in the trailing part of the active region. The force-free parameter α was iteratively tuned so as to obtain a general fit between the orientations of the flare loops observed by TRACE and of the calculated field lines rooted in the vicinity of these loops. This constraint led to fixing $\alpha = -5\times10^{-3}$ Mm^{-1}, whose sign is compatible with the hemispheric helicity rules found by Pevtsov et al. (1995).

Even though the results of this calculation were used to study the triggering and the development of the flare, we must point out that they are uncertain for two reasons. Firstly, the selected α is equal to 80% of the resonant value well known for extrapolations performed with a FFT in a large computational box. This leads to a very probable artificial over-shearing of the large scale loops. Secondly, it was impossible to find a single value of α with, even in a 20% interval, which allowed us to fit all the observed TRACE loops with calculated magnetic field lines. Therefore, it appears that the $\alpha = \mathrm{cst}$ hypothesis of the *lfff* extrapolation may be strongly disputed in this region. Nevertheless, as the global magnetic topology is a well preserved property of magnetic fields since it is an integral quantity, we still used the *lfff* model to pursue our analysis, although it is clear that it is disputable on small scales (where electric currents are concentrated) and on large scales (where the field is too sheared).

3.2. Origins of the asymmetrical ribbons

Figure 11 shows the results of the *lfff* extrapolation. The large-scale shear is evident on the scale of the full active region, as seen in the *top left* panel. The other panels show the connectivities of the magnetic field lines in the vicinity of the emerging bipole and around the flare ribbons as observed in Hα.

In this region, even though a few nulls points are present around the negative moving magnetic features on the edges of the leading spot, the global topology is *not* complex: no thin quasi-separatrix layers were found to be associated with the flare loops, contrary to many previous studies of confined flares (see, e.g., Mandrini et al. 1996; Schmieder et al. 1997; Aulanier et al. 2000). Also, the connectivities look very continuous around the region of the emerging bipole, so at first sight it appears that the flare studied in this paper cannot be interpreted with the standard reconnexion model. However emerging bipoles are known to often emerge twisted (Leka et al. 1996; Lopez-Fuentes et al. 2000), which is supported by the Huairou vector magnetograms for this region (Y. H. Yan, private communication). Therefore we conjecture that the flare was still probably due to magnetic reconnection, but here between small-scale twisted emerging fields (not calculated in the extrapolation) and the large-scale sheared magnetic fields of the global bipole of NOAA 0162. Since the flare was confined, it may then be interpreted by the global disruption model calculated by Amari et al. (1999) in a very symmetrical configuration, where a locally twisted flux tube undergoes an ideal kink instability and reconnects with overlaying potential fields.

If we assume the global disruption scenario, the *lfff* model naturally provides an explanation for the appearance of the compact ribbon R1 and its elongated counterpart R2, as well as its fast propagation away from the emerging bipole and toward the leading sunspot. Figure 11 indeed shows that the field lines located higher and higher above the emerging bipole are rooted in R1 and R2, and have footpoint separations that are small on the R1 side and quite large on the R2 side. The continuous reconnection of the growing emerging fields with higher and higher overlaying fields provides a natural explanation for the sequential brightening of their footpoints along the flare ribbons, included along the very elongated R2 ribbon. In this framework, the fast propagation of the brightenings as observed by TRACE are not due to MHD waves, but are rather due to the electron beams accelerated from the reconnection regions above the emerging bipole in the long overlaying loops of NOAA 0162, which progressively reach larger and larger chromospheric areas toward the West.

It is also noteworthy that the shape of the field lines anchored in the Hα ribbons follows the elongated shape of the RHESSI images recorded in the 6–12 keV range of energy between 16:03–16:09 UT. Thus, the extrapolation supports the idea that RHESSI observes thermal emission of coronal loops heated by the confined flare. It is, however not contradictory that the RHESSI also detect a non-thermal component since its is known that reconnection can accelerate particles along reconnected field lines. The RHESSI emission at 16:25–16:28 UT being similar in shape to the one recorded at 16:03–16:09 UT, though slightly shifted southward, suggests that this secondary event may be associated with the resistive relaxation of the system which may have been forced too rapidly by the flare of 15:59 UT, as in the reconnection calculations of Karpen et al. (1998). Unfortunately, the present data and model cannot provide more clues to this issue.

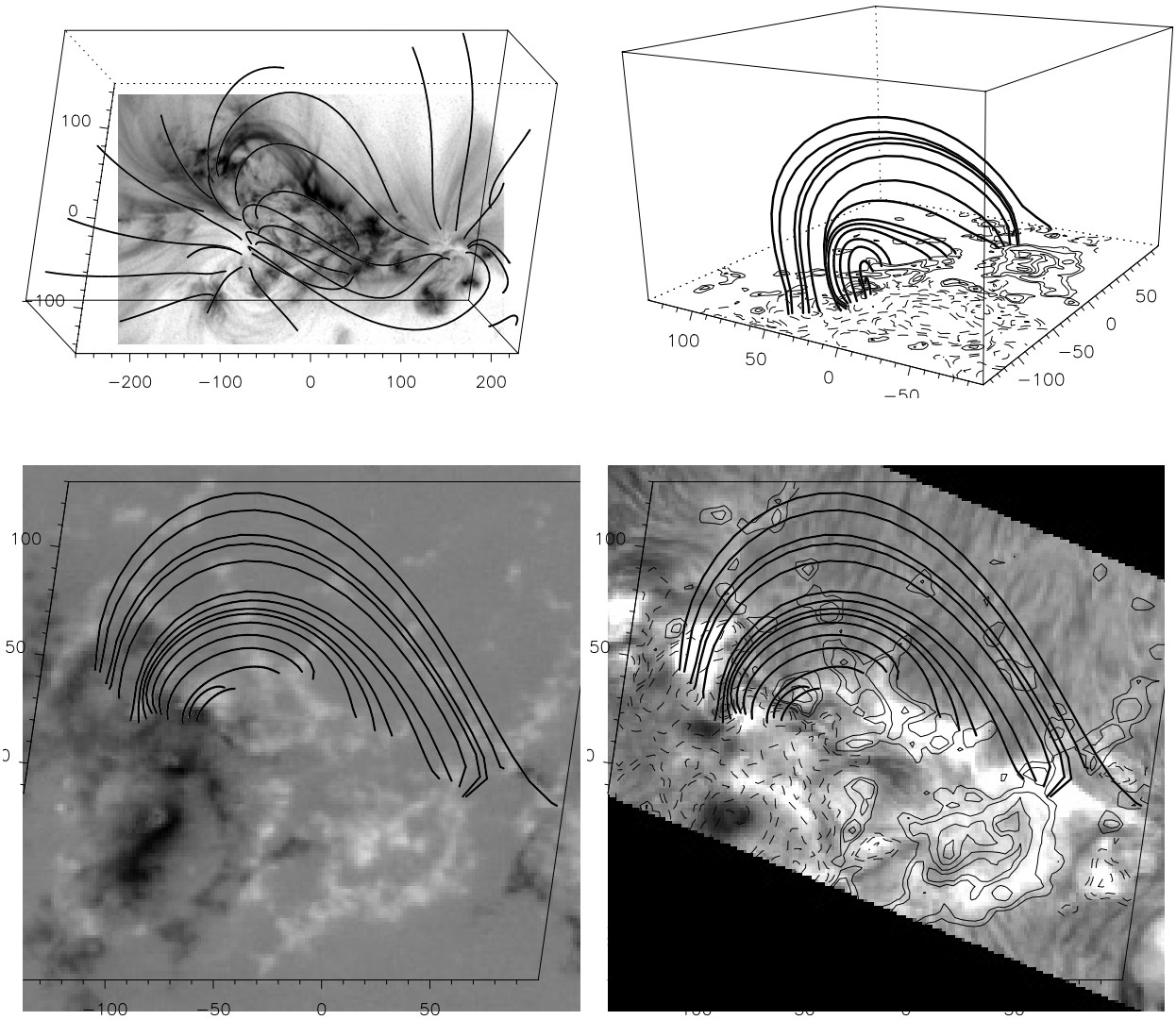

Fig. 11. *Top left*: superposition of the TRACE 195 Å image of 16:59 UT with a sample of magnetic field lines resulting from the *lfff* extrapolation. *Top right*: projection view of the field lines shown in the *bottom* panels. Continuous (resp. dashed) contours stand for positive (resp. negative) vertical fields. North is toward the left. *Bottom right*: partial view of the flare as observed in Hα with the VTT/MSDP at 16:00 UT. The field lines are the ones which are rooted in the flare ribbons R1 and R2 as well as in the emerging bipole. *Bottom left*: same as *bottom right*, except that the underlying image is the THEMIS Na D_1 magnetogram at 12:32 UT.

4. Thermal and non-thermal component in the gradual phase

Using RHESSI data and the SPEX package we performed spectral analysis of X-ray emission from 16:03 to 16:27 UT. The background emission was evaluated using data taken before the flare during the previous RHESSI orbit between 15:12 and 15:24 UT. Spectral accumulation was done for all 1 min time bins between 16:03 and 16:27 UT and was performed using 0.25 keV energy bins in the 3–10 keV energy range and 1 keV energy bins above 10 keV. To obtain the spectra we used the front segments of detectors 1F–9F (except 2F and 7F.) We omitted the data from these detectors because they have a poorer energy resolution than intended (Smith et al. 2002). We performed the full calculation of all diagonal and off-diagonal matrix elements.

All the spectra accumulated between 16:03 and 16:27 UT were analysed with SPEX. To reproduce the observed count spectra, we used a model consisting a thermal component (characterized by an emission measure and a temperature) and a power-law non-thermal component. In addition to these continuum components we considered two lines that Phillips (2004) predicted to be significant in X-ray spectra observed by RHESSI for hot ($T_e > 10$ MK) plasma. The first line is a Fe-line feature at ~6.7 keV and the second line is a Fe/Ni complex line feature at ~8 keV emitted from even hotter plasma. The 6.7 keV feature corresponds mainly to the Fe XXV lines and associated dielectronic satellites, centred on 6.6 keV and to Fe XXVI lines and associated satellites, centred on 6.9 keV. The 8 keV line feature is due to Fe XXV and Fe XXVI lines as well as Ni XXVII and Ni XXVIII lines. The lines are excited at electron $T_e > 10$ MK. The contributions of individual lines to the

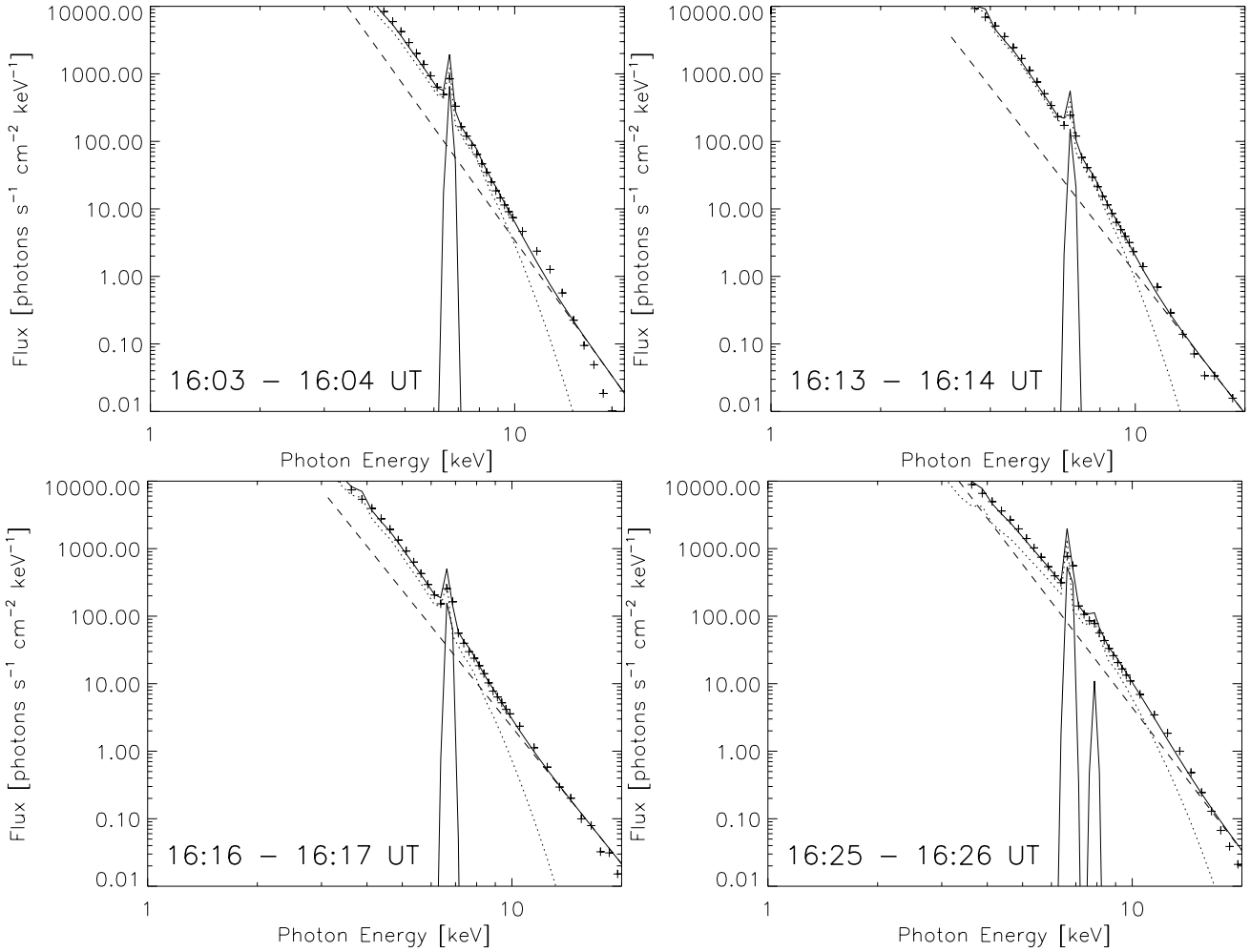

Fig. 12. RHESSI spectra reconstructed during the gradual phase of the solar flare in four intervals: 16:03–16:04, 16:13–16:14, 16:16–16:17 and 16:25–16:26 UT. Dotted lines denote the calculated thermal component, dashed lines represent non-thermal component, thin continuous lines are the Fe-line feature (~6.7 keV) calculated in our model. In our modelling of the spectrum at 16:25–16:26 UT we also used the Fe/Ni-line feature (~7.9 keV). Thick continuous lines are the sum of all components-predicted photon spectrum. With crosses we marked observed flare spectrum. The temperature of plasma T, emission measure EM, power-law index of non-thermal component γ, and normalization of broken power-law A at 10 keV for these spectra are: 16:03–16:04 UT: $T1$ = 9.8 MK, $EM1 = 2.3 \times 10^{48}$ cm^{-3}, $\gamma 1 = -7.5$, $A1$ = 3.3 photons s^{-1} cm^{-2} keV^{-1}; 16:13–16:14 UT: $T2$ = 9.1 MK, $EM2 = 1.5 \times 10^{48}$ cm^{-3}, $\gamma 2 = -6.9$, $A2$ = 1.1 photons s^{-1} cm^{-2} keV^{-1}; 16:16–16:17 UT: $T3$ = 9.4 MK, $EM3 = 9.4 \times 10^{47}$ cm^{-3}, $\gamma 3 = -6.7$, $A3$ = 2.1 photons s^{-1} cm^{-2} keV^{-1}; 16:25–16:26 UT: $T4$ = 13.7 MK, $EM4 = 2.4 \times 10^{47}$ cm^{-3}, $\gamma 4 = -7.0$, $A4$ = 4.1 photons s^{-1} cm^{-2} keV^{-1}.

total emission within both line features is temperature dependent (Phillips 2004). The Fe/Ni-line feature starts to be visible with RHESSI at higher temperatures than Fe-line feature, and for the $T_e < 20MK$ the Fe/Ni-line feature is very weak.

Figure 12 shows the photon spectrum resulting from the fitting of the model to the observed count spectrum within the 3–20 keV energy range. For all spectra a non-thermal continuum is necessary to reproduce the observation above 10 keV. Furthermore, for all spectra the Fe-line feature at ~6.7 keV is seen in the count and photon spectra. For the spectra after 16:25 UT, the complex Fe/Ni-line feature at ~8 keV gives a marginally significant contribution to the observed spectrum consistent with the higher temperatures deduced from the thermal component. The main difference in the spectra obtained between 16:03 and 16:27 UT is the increase of the temperature of the thermal component at 16:26 UT as well as the contribution of the non-thermal component to the spectra above 10 keV. The contribution of the non-thermal component (see Fig. 12) is larger in the 16:16–16:17 UT and 16:25–16:26 UT, during time intervals corresponding to some additional increases of the X-ray flux in 12–25 keV energy range. In the figures the fitted spectra are shown assuming no low energy cut-off for the non-thermal part of the photon spectrum. The effect of a low energy cut-off around 10 keV for the non-thermal photon spectrum were analysed. Below the cut-off we assumed a photon spectrum with an index of −1.5. We found that below 10 keV the fit is not strongly dependent on the existence and the value of this cut-off which means that the thermal emission is dominant below 10 keV. For all spectra and independent on the cut-off value the contribution of a non-thermal component is necessary to explain the photon spectrum between 10 and 20 keV.

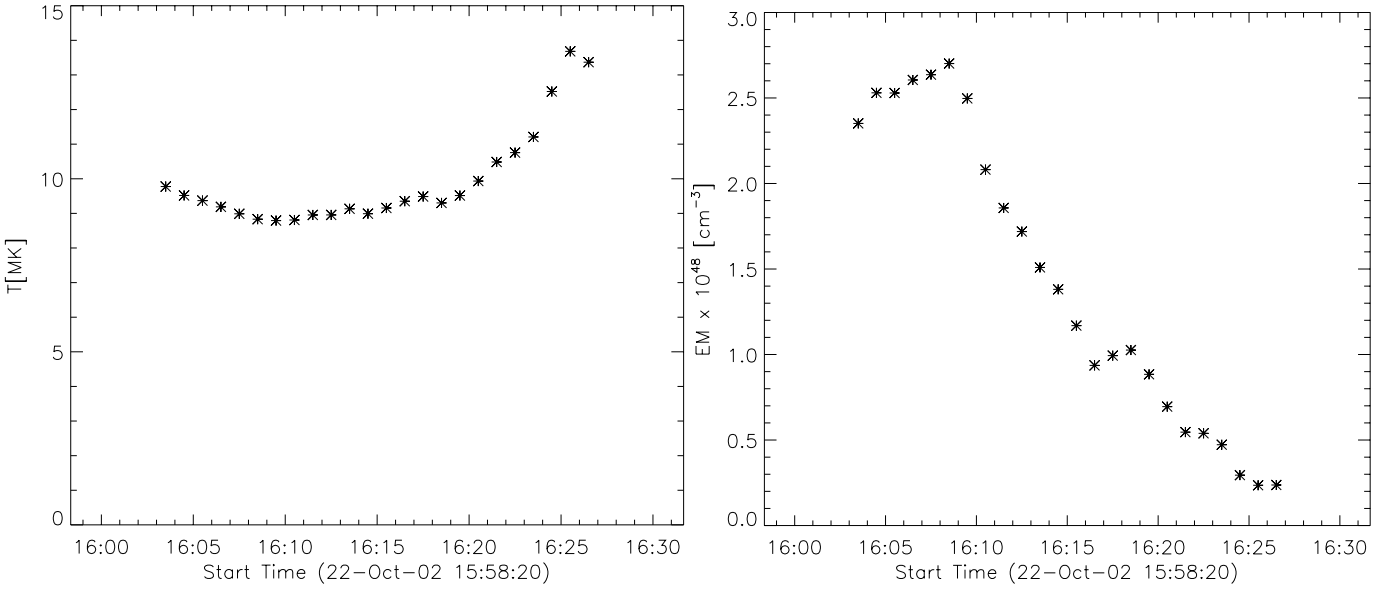

Fig. 13. The time evolution of the temperature T and emission measure EM of the flare on October 22, 2002 These parameters were obtained from fitting the observed RHESSI spectra with the model.

Table 1. Thermal $E_{\rm th}$ and non-thermal $E_{\rm nth}$ energy contained in the flare of October 22, 2002.

Time (UT)	$E_{\rm th}$ (erg)	$E_{\rm nth}$ (erg)	$E_{\rm nth}/E_{\rm th}$ (%)
16:03	6.3×10^{29}	2.1×10^{26}	0.03
16:15	1.6×10^{29}	7.9×10^{25}	0.05
16:25	1.2×10^{29}	3.6×10^{26}	0.30

Figure 13 shows the time evolution of the temperature T and emission measure EM obtained by the fitting of the observed count spectra with the model. First, the deduced temperature decreases from about 9.7 MK to 8.8 MK and after, at 16:10 UT starts to increase to the value of 13.6 MK. It means that from about 16:10 UT some additional heating processes took place. The maximum value of the temperature at 16:25 UT is consistent with the marginal appearance of the Fe/Ni-line feature at the same time. Between 16:03 and 16:09 UT the emission measure exhibited some increase. At about 16:09 UT EM started to decrease from 2.53×10^{48} cm^{-3} to 2.35×10^{47} cm^{-3} at 16:27 UT that indicates a continuous decrease of the amount of emitting plasma.

We performed a simple calculation to estimate how much energy is stored in non-thermal electrons compared to the thermal energy of the flare. The thermal energy contained in a high-temperature plasma is given by $E_{\rm th} = 3nkTV$, where n is the mean (neglecting the filling-factor) plasma density, T – temperature, and V is the volume of the flaring plasma. We use RHESSI images to estimate V. The emission measure can be written as $EM = \int_V n^2 \, {\rm d}V$. In the case of homogeneous plasma the density of the plasma is $n = (EM/V)^{1/2}$. The emission measure and the temperature were obtained from RHESSI spectra analysis. Transforming the previous equation for E_{th} into the form $E_{\rm th} = 3kT(EM \cdot V)^{1/2}$ we calculated thermal energy of the flare at three times: 16:03, 16:15 and 16:25 UT.

The energy stored in non-thermal electrons can be obtained using the method described in Hudson et al. (1978). We use the thin-target model because we observe the soft X-ray emission in the top parts of the flare loops where the plasma density is not as high as in the loop footpoints. We took into account all non-thermal electrons with energy ≥10 keV and we used the modified formula for the energy stored in these electrons:

$$E_{\rm nth} = 5.21 \times 10^{35} \frac{\gamma - 1}{(\gamma - \frac{5}{2}) B(\gamma - 1, \frac{1}{2})} \frac{\Phi_{10}}{n} \ \ [\rm erg], \qquad (1)$$

where γ is the power-law index of the X-ray spectrum, $B(x, y)$ – the beta function, Φ_{10} – the X-ray spectral flux [photons cm^{-2} s^{-1} keV^{-1}] at 10 keV as derived from the observations, and n is the value of plasma density. In Table 1 we present the values of thermal and non-thermal energy at the three times during the flare. We also give the ratio (in %) of both energies. At all three times the energy contained in the non-thermal electrons is significantly smaller compared to the thermal energy of flaring plasma. The values of thermal energy are consistent with the results published for other flares (McDonald et al. 1999).

During the analysed period (16:03–16:28 UT) the thermal energy of flaring plasma is dominant. The non-thermal electrons provide a marginal input to the total energy of the flare but are still necessary to explain the non-thermal component observed in the RHESSI spectra. During the X-ray flux rise observed at 16:25 UT the energy contained in non-thermal electrons is significantly higher but not sufficient to explain the thermal energy radiated during this time.

5. Conclusions

In this paper we performed an analysis of the morphology and evolution of an M 1.0 flare on October 22, 2002 observed mainly during its gradual phase. We used multi-wavelength observations obtained in the optical range as well as in X-ray and

EUV. We also analysed the line-of-sight magnetic field of the AR 0162 which allowed us to understand the mechanisms responsible for the observed evolution of this event. The magnetic field (photospheric and extrapolated) and the aligned Hα ribbons shows that this active region was highly sheared, thus was storing energy. The triggering of Hα flare occurs in a region of a high gradient of B which could correspond to the emergence of locally very twisted magnetic flux. The *lfff* extrapolation of the magnetic field provides an explanation for the appearance two Hα flare ribbons: ribbon R1 was compact and its position was almost constant during the flare; ribbon R2 was elongated and exhibited fast propagation along it, from the emerging bipole towards the leading sunspot. This propagation can be explained by the reconnection of the growing emerging field lines with a higher and higher overlying field. The shift of RHESSI X-ray and CDS/EUV emission observed with time above the AR also confirms the idea of subsequential reconnection of magnetic field lines. The elongated shape of X-ray and EUV structures observed during the gradual phase follow the shape of the magnetic field lines anchored in the Hα ribbons. Thus, we can say that RHESSI and CDS permit us to see the thermal emission of successive coronal loops heated probably by non-thermal electrons, accelerated by reconnection processes during the impulsive phase of this flare.

The presence of a non-thermal component during the gradual phase of flares is still not clear. It is well known that non-thermal particles occur during the impulsive phase of flares and they can still exist during the late phase of an eruptive flare. Analysis of magnetic field configuration showed that the flare of October 22, 2002 was of the confined type. During this event we did not observe either CME or any other signatures of an eruption. The presence of non-thermal particles can be deduced from the X-ray spectra reconstructed during the gradual phase; indeed RHESSI spectra show that the non-thermal component is necessary to explain the spectra between 10 and 20 keV but the emission below 10 keV observed during gradual phase is mainly of thermal origin. During the analysed period the energy contained in the non-thermal electrons is however negligible compared to the thermal energy of flaring plasma.

From the RHESSI spectra we found the temperature of the flare plasma to be around 8.5–14 MK. This is typical for the structures observed during the gradual phase of solar flares. The Fe-line feature (~6.7 keV) also indicates the presence of high temperature plasma (about 9–10 MK) (Phillips 2004). At 16:26 UT, during the increase of X-ray flux, we also observed Fe/Ni-line feature (~7.9 keV). The presence of this line emission is due to a temperature increase to about 14 MK. The CDS observations in the Fe XIX flare line (592.2 Å) confirm the existence of hot plasma of that temperature. The Fe XIX emission arises at around 8–9 MK which is in agreement with the temperatures obtained from the RHESSI spectra. The Fe XIX emission was nearly co-spatial with the RHESSI X-ray emission.

The high plasma temperatures observed during the gradual phase of this flare are in agreement with the commonly-accepted model for gradual phase of flares (Forbes & Malherbe 1986; Forbes & Acton 1996). During the decay phase, X-ray emission was observed at the reconnection site of the magnetic field lines. The X-ray and EUV observations suggest that this emission originated from continuous reconnection processes rather than from trapped particles. There was no X-ray emission at the footpoints of the loops which indicates that during the gradual phase, non-thermal heating of Hα flare ribbons was not present. Thermal conduction heating can be responsible for the flare ribbons observed by TRACE but is not sufficient to explain the Hα flare emission (Berlicki & Heinzel 2004). We need to investigate other processes (for instance the effect of high coronal pressure).

Acknowledgements. The magnetic field extrapolations used in this paper were obtained from the code base FRench Online MAGnetic Extrapolations (FROMAGE). FROMAGE is a joint project between LESIA (Observatoire de Paris), CPhT (École Polytechnique) and the Centre National d'Études Spatiales (CNES). The work of A.B. was supported by the European Commission through the RTN programme (European Solar Magnetism Network, contract HPRN-CT-2002-00313). VTT/MSDP observations have been provided and reduced by P., N. Mein and J. Staiger. These observations were performed during a MEDOC campaign (JOP 157). G.D.Z. acknowledges support from PPARC (UK). The TRACE analysis at SAO is supported by a contract from Lockheed Martin. The authors are grateful to the RHESSI Team (PI: R. P. Lin) for the free access to the RHESSI data and the development of the software. MDI and CDS data were provided by SoHO consortium. SoHO is a joint project of ESA and NASA. N.V. would like to acknowledge many useful discussion on RHESSI imaging techniques and spectroscopy with R. P. Lin, G. Hurford, S. Krucker and R. A. Schwartz. The support of CNES to the RHESSI project is also acknowledged.

References

Alissandrakis, C. E. 1981 A&A, 100, 197
Amari, T., & Luciani, J. F. 1999, ApJ, 515, L81
Aulanier, G., DeLuca, E. E., Antiochos, S. K., McMullen, R. A., & Golub, L. 2000, ApJ, 540, 1126
Berlicki, A., & Heinzel, P. 2004, A&A, 420, 319
Del Zanna, G., & Mason, H. E. 2003, A&A, 406, 1089
Del Zanna, G., Bromage B. J. I. E., Landi, E., & Landini, M. 2001, A&A, 379, 708
Del Zanna, G., Mason, H. E., Gibson, S. E., Pike, C. D., & Mandrini, C. H. 2002a, Adv. Space Res., 30(3), 551
Del Zanna, G., Mason, H. E., & Foley, C. 2002b, Proc. 10th European Sol. Phys. Meet., ESA-SP 506, 585
Démoulin, P., Bagala, L. G., Mandrini, C. H., Henoux, J. C., & Rovira, M. G. 1997, A&A, 325, 305
Eibe, M. T., Aulanier, G., Faurobert, M., Mein, P., & Malherbe, J. M. 2002, A&A, 381, 290
Forbes, T. G., & Acton, L. W. 1996, ApJ, 459, 330
Forbes, T. G., & Malherbe, J. M. 1986, ApJ, 302, L67
Handy, B. N., Acton, L. W., Kankelborg, C. C., et al. 1999, Sol. Phys., 187, 229
Harrison, R. A., Sawyer, E. C., Carter, M. K., et al. 1995, Sol. Phys., 162, 233
Hudson, H. S., Canfield, R. C., & Kane, S. R. 1978, Sol. Phys., 60, 137

Karpen, J. T., Antiochos, S. K., Devore, C. R., & Golub, L. 1998, ApJ, 495, 491
Kopp, R. A., & Pneuman, G. W. 1976, Sol. Phys., 93, 351
Leka, K. D., Canfield, R. C., McClymont, A. N., & van Driel-Gesztelyi, L. 1996, ApJ, 462, 547
Lin, R. P. 2002, Sol. Phys., 210, 3
Lopez Fuentes, M. C., Démoulin, P., Mandrini, C. H., & van Driel-Gesztelyi, L. 2000, ApJ, 544, 540
Mandrini, C. H., Démoulin, P., van Driel-Gesztelyi, L., et al. 1996, Sol. Phys., 168, 115
McDonald, L., Harra-Murnion, L. K., & Culhane, J. L. 1999, Sol. Phys., 185, 323
Mein, P. 1991, A&A, 248, 669
Mein, P. 2002, A&A, 381, 271
Pevtsov, A. A., Canfield, R. C., & Metcalf, T. R. 1995, ApJ, 440, L109
Phillips, K. J. H. 2004, ApJ, 605, 921
Schmieder, B, Heinzel, P., van Driel-Gesztelyi, L., & Lemen, J. R. 1996, Sol. Phys., 165, 303
Schmieder, B., Aulanier, G., Démoulin, P., et al. 1997, A&A, 325, 1213
Semel, M. D. 1967, Ann. Astroph., 381, 271
Smith, D. M., Lin, R. P., Turin, P., et al. 2002, Sol. Phys., 210, 33
Švestka, Z. 1986, in The Lower Atmosphere in Solar Flares, NSO, 332
Švestka, Z., Hoyng, P., van Tend, W., et al. 1982, Sol. Phys., 75, 305
van Driel-Gesztelyi, L., Wiik, J. E., Schmieder, B., et al. 1997, Sol. Phys., 174, 151